Measurement and Prediction of Damage Threshold of Gold Films During Femtosecond Laser Ablation

T. Balasubramani, S. H. Kim and S. H. Jeong

Gwangju Institute of Science and Technology (GIST)

ABSTRACT

The damage threshold measurement of gold films is carried out with ultrashort-pulse laser. An enhanced two temperature model is developed to encounter the limitation of linear modeling during ultrashort pulse laser ablation. In which the electron heat capacity is calculated using a quantum mechanical approach based on a Fermi-Dirac distribution, temperature-dependent electron thermal conductivity valid beyond the Fermi temperature is adopted, and reflectivity and absorption coefficient are estimated by applying a temperature-dependent electron relaxation time. The predicted damage threshold using the proposed enhanced modelclosely agreed with experimental results, demonstrating the importance of considering transient thermal and optical properties in the modeling of ultrashort pulse laser ablation.

Key Words: Two temperature model, electron heat capacity, damage threshold fluence

1. Introduction

The interactions of ultrashort pulse laser and materials have demonstrated the advantages over nanosecond lasers in various fields for which a more comprehensiveunderstanding of laser-material interactions is required. The energy transfer mechanisms during ultrashort pulse laser interactions with materials play a key role and the resulting effects on target materials are significantly different from those in nanosecond laser ablation. An intense femtosecond laser pulse can lead to ablation of materials at much lower laser fluences than long pulse lasers[1-3] and produce micromachined structures with minimal melting effects[2,4]. The ultrashort pulse laser and metals interaction can be described by two temperature model (TTM) which was proposed by Anisimov et al.[5] Since then, various theoretical and experimental studies have been conducted in attemptsto explain the laser energy coupling with materials that occurs during femtosecond laser ablation. For example, Stuart et al.[3] showed that the damage threshold fluence of gold mirrors and gratings decreased with a $\tau^{1/2}$-dependence down to a pulse of 200 ps, where τ is the laser pulse duration, but remained nearly constant for shorter pulses (λ = 1053 nm). The measured damage threshold for varying film thicknesses using a 600 fs pulse showed that thedamage threshold of gold films first increased linearly with film thickness, but then became independent of thickness for films thicker than the thermal penetration depth. Wellershoff et al.[6] reported similar results from the damage threshold measurements of gold films using an ultrashort pulse laser (τ = 200 fs, λ = 400 nm) for varying film thicknesses. In which, the damage threshold of gold films increased linearly with film thickness up to a thickness close to the electron diffusion length (L_e), which is related to the electron-phonon coupling constant (G) and the melting temperature (T_m) by $L_e \sim (G^2 T_m)^{-1/4}$, but for films thicker than L_e the threshold became saturated

at the value of about 0.11 J/cm^2. The authors also compared the measured and calculated threshold fluences for varying pulse durations and emphasized the need to take into account transient optical properties in the theoretical modeling of ultrashort pulse laser ablation. In the theoretical fronts, several modified TTMs have also been proposed for a more rigorous analysis[6-8]. The widely-used expression for electron heat capacity in conventional TTMs $C_e(T_e)=\gamma T_e$ with $\gamma=\pi^2 k_B^2 n_e/2\varepsilon_F$[9,10], where γ is the electron heat capacity constant, k_B is the Boltmann constant, n_e is the density of free electrons, ε_F is the Fermi energy, and T_e is the electron temperature, is an approximation based on the assumption that the temperature of interest is far less than the Fermi temperature, 6.39 × 10^4 K[10]. Similarly, the expression $k_e(T_e,T_i)=k_0 T_e/T_l$[11] for electron thermal conductivity, where T_l is the lattice temperature and k_0 is the value at thermal equilibrium between electrons and phonons, is also limited to temperatures much lower than the Fermi temperature. Moreover, optical properties are often taken as constant values at room temperature in conventional TTMs; for example, the reflectivity and optical penetration depth of gold were assumed to be 0.97 and 13.7 nm, respectively[12].

In this work, a quantum mechanical approach for TTMs in which temperature-dependent electron thermal properties and transient optical properties are employed is proposed. The electron heat capacity is calculated based on a Fermi-Dirac distribution and ageneral expression for electron thermal conductivity[11,13,14], derived from the first principle, is adopted so that the calculation can be extended beyond the Fermi temperature. Reflectivity and absorption coefficient of the target are then represented as functions of electron relaxation time. Using this enhanced TTM, the ultrashort pulse laser ablation of gold films coated on a glass substrateis investigated and compared with experimental results.

2. Two temperature model

The temperatures of electron and lattice subsystems during ultrashort pulse laser ablation are expressed by the following equations

$$C_e(T_e)\frac{\partial T_e}{\partial t}=\frac{\partial}{\partial z}\left(k_e(T_e)\frac{\partial}{\partial z}T_e\right)-G(T_e-T_l)+S(z,t)$$

$$C_l\frac{\partial T_l}{\partial t}=G(T_e-T_l)$$

where C is the specific heat capacity, z is the distance measured from the surface into the film, t is time, k is the thermal conductivity, and G is the electron-phonon coupling factor. The subscripts e and l represent the electron and phonon, respectively. The source term represents the incident laser light and is expressed by

$$S(z,t)=[1-R(T_e)]I_0\exp\left[-\frac{|t-t_0|^2}{(0.5\tau_p)^2}\right]\alpha(T_e)\exp[-\alpha(T_e)z]$$

where I_0 is the laser irradiance, τ_p is the pulse width at $1/e$ of the peak irradiance, t_0 is the time at which the peak intensity R is located, α is reflectivity, and is the absorption coefficient.

The limitations of the conventional two-temperature model arise from the simplification of the expressions for thermal and optical properties; for example, the linear expressions $C_e(T_e)=\gamma T_e$ where γ is a constant and $k_e(T_e,T_l)=k_0 T_e/T_l$ are frequently adopted for simplicity with constant optical properties. To overcome these limitations, we employed more rigorous expressions for thermal and optical properties in the two-temperature model. First, the electron heat capacity is directly calculated by the numerical integration of electron kinetic energy using the following expression[10,15,16]

$$C_e(T_e)=n_e\left(\frac{\partial<\varepsilon>}{\partial T_e}\right)_V \quad (1)$$

where n_e is the electron number density, ε is the kinetic energy of a free electron, and V is

volume. The average kinetic energy per electron is given by

$$<\varepsilon>=\frac{\sum_k <n_k\varepsilon_k>}{N_e}=\frac{\int_0^\infty \frac{1}{e^{\beta(T_e)[\varepsilon-\mu(T_e)]}+1}\rho(\varepsilon)\varepsilon\, d\varepsilon}{\int_0^\infty \frac{1}{e^{\beta(T_e)[\varepsilon-\mu(T_e)]}+1}\rho(\varepsilon)\, d\varepsilon}$$

where $<n_k>=\frac{1}{e^{\beta(T_e)[\varepsilon_k-\mu(T_e)]}+1}$, $\beta(T_e)=\frac{1}{k_B T_e}$, $\rho(\varepsilon)=\frac{8\sqrt{2}\pi m_e^{3/2}\sqrt{\varepsilon}}{h^3}$ and the chemical potential[9] is

$$\mu(T_e)=\varepsilon_F\left[1-\frac{\pi^2}{12}\left(\frac{k_B T_e}{\varepsilon_F}\right)^2-\frac{3\times 7\pi^4}{8\times 360}\left(\frac{k_B T_e}{\varepsilon_F}\right)^4\right].$$

Equation (1) can be reduced to $C_e(T_e)=\gamma T_e$ if the electron temperature can be assumed to be less than $0.01T_F$ and $\mu=\varepsilon_F$. The phonon heat capacity (C_l) is taken to be constant. For thermal conductivity, the expression based on first principle is adopted[11,13,14] to cover electron temperatures beyond the Fermi temperature as

$$k_e(T_e,T_l)=K\frac{\left(\theta_e^2+0.16\right)^{5/4}\left(\theta_e^2+0.44\right)^{5/4}\theta_e}{\left(\theta_e^2+0.092\right)^{1/2}\left(\theta_e^2+b\theta_l\right)} \qquad (2)$$

where $\theta_e=k_B T_e/\varepsilon_F$, $\theta_l=k_B T_l/\varepsilon_F$, and K and b are materials specific constants.

Reflectivity and absorption coefficient are calculated from the real (n) and imaginary (κ) parts of the refractive indices as

$$R=\frac{[n-1]^2+\kappa^2}{[n+1]^2+\kappa^2} \quad \text{and} \quad \alpha=\frac{4\pi\kappa}{\lambda}$$

where n and κ are estimated from the complex dielectric constant expressed by[17]

$$\varepsilon_r=\varepsilon_1+i\varepsilon_2=1+\frac{n_e e^2}{m_e\varepsilon_0}\left(\frac{-\tau_e^2+i\tau_e/\omega}{1+\omega^2\tau_e^2}\right)$$

where ω is the laser frequency and τ_e is the relaxation time calculated using the definition of thermal conductivity[10] as

$$\tau_e(T_e,T_l)=\frac{3k_e(T_e,T_l)}{C_e(T_e)v_e^2}$$

where v_e^2 is the mean square of the electron speed[15] and k_e was calculated using Eq. (2).

3. Experiments

For a comparison of the theoretical prediction from the enhanced TTM withthe experimental results, measurement of damage threshold was carried out with gold (purity of 99.99%) films deposited on fused silica substrates. The ablation was performed under atmospheric pressure with a chirped-pulse amplification Ti:sapphire laser system (Cyber Laser Inc., FS-IFRIT, Gaussian profile, repetition rate=1 kHz) pulse duration and wavelength were 184 fs and 785 nm, respectively. Here, the laser pulse energy of each incident light was adjusted using a half-wave plate and a linear polarizer, and measured with a pyroelectric detector. A Pockels cell was utilized to control the pulse numbers both single- and multi(20)-pulse irradiation were used to determine the threshold measurement. The original beam diameter was 8.5 mm, and to obtain a more uniform energy distribution at the target surface an aperture with a 4.4 mm diameter was placed in the beam path. Prior to measurement, the target gold films were mounted on a computer-controlled three-axis translation stage and placed at the focal plane of an achromatic focusing lens (f=200 mm). Gold films of varying thicknesses were prepared with an electron-beam evaporator and the thickness of each gold film was then measured using an atomic force microscope.

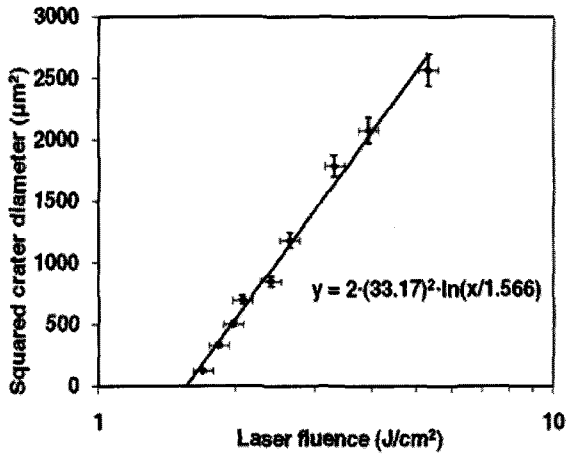

Fig. 1 Measured crater diameters as a function of laser fluence.

For accurate determination of the damage threshold fluences, the spot diameter of the laser beam at the target surface needs to be known. For this purpose, the gold films were ablated for varying laser fluences (from high fluence of 5.3 J/cm^2 to low fluence of 1.3 J/cm^2 and the following linear relationship between the squared crater diameter and laser beam fluence[18,19] was utilized to estimate the spot radius.

$$D^2 = 2\omega_0^2 \ln\left(\frac{F_0}{F_{th}}\right), \quad F_0 = \frac{2E_p}{\pi\omega_0^2} \tag{3}$$

where D is the measured crater diameter, ω_0 is the $1/e^2$-radius of the incident beam at the target surface, F_{th} is the threshold fluence, and E_p is the incident laser pulse energy. Using Eq. (3), the measured crater diameter (D^2) could then be plotted with respect to either the laser pulse energy (E_p) or the laser fluence (F_0) in the logarithmic scale, as shown in Fig. 1. The slope of this graph provides the spot radiusof the incident laser beam; from the figure, ω_0 was estimated to be 33.2 μm.

The determination of the damage for each film after laser ablation was conducted by detecting color or morphological changes of the irradiated surface using a scanning electron microscope (SEM). Here, visible changes of the surface were used as the criterion for threshold determination, and thus weak ablation effects such as melting of a very thin layer, local structural defects, or a small amount of ablation may have been missed; as a result, theexperimentally-determined damage threshold values are expected to be slightly higher than the minimum fluence at which those weak physical changes may occur. Figure 2 shows the sample SEM images of gold films of different thicknesses ablated at 1.29 J/cm^2 for a 300 nm thick film [Fig. 2(a)], 1.22 J/cm^2 for a 250 nm thick film [Fig. 2(b)], 1.13 J/cm^2 for a 200 nm thick film [Fig. 2(c)], 1.04 J/cm^2 for a 150 nm thick film [Fig. 2(d)], 0.51 J/cm^2 for a 50 nm thick film [Fig. 2(e)], and 0.23 J/cm^2 for a 20 nm thick film [Fig. 2(f)]. For the relatively thick film in Fig. 2(a), a color change over the irradiated area was visible; accordingly, the damage threshold was determined. For thin films, however, for example, the 20 nm-thickfilm in Fig. 2(c), the irradiated film was almost entirely ablated from the substrate if a visible damage occurred. For the intermediate thicknesses, damage was observed in various forms such as a local crack, as shown in Fig. 2(b), partial ablation at the center of the irradiated region, or a local bump, and was used to determine the threshold. This method of damage determination was subsequently applied to both single-pulse and multi-pulse ablation experiments, the results of which are presented in Section 4 along with the calculation data. The Fig. 3 shows SEM images of gold films of different thicknesses for multi(20)-pulse ablation at 0.995 J/cm^2 for a 250 nm thick film [Fig. 3(a)], 0.926 J/cm^2 for a 200 nm thick film [Fig. 3(b)], 0.712 J/cm^2 for a 100 nm thick film [Fig. 3(c)], 0.207 J/cm^2 for a 20 nm thick film [Fig. 3(d)]

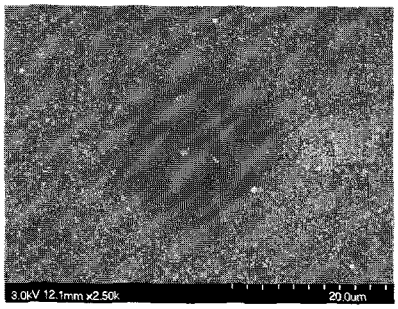

(a)

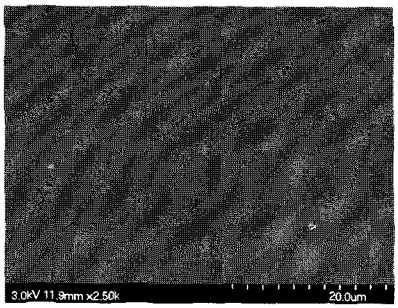

(b)

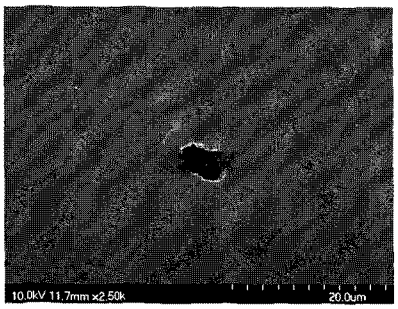

(c)

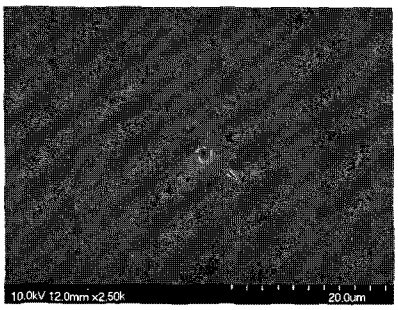

(d)

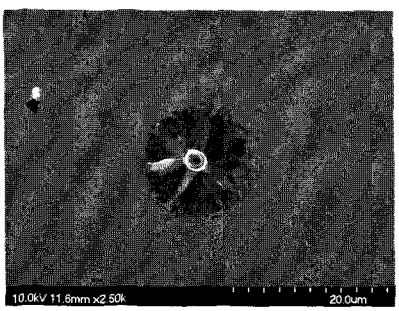

(e)

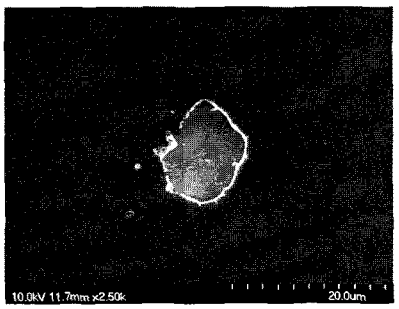

(f)

Fig. 2 SEM images of Au films ablatedby 184-fs laser single pulse. The laser fluences and film thicknesses were (a) 1.29 J/cm^2 for 300 nm (b) 1.22 J/cm^2 for 250 nm, (c) 1.13 J/cm^2 for 200 nm, (d) 1.04 J/cm^2 for 150 nm, (e) 0.51 J/cm^2 for 50 nm, and (f) 0.23 J/cm^2 for 20 nm, respectively.

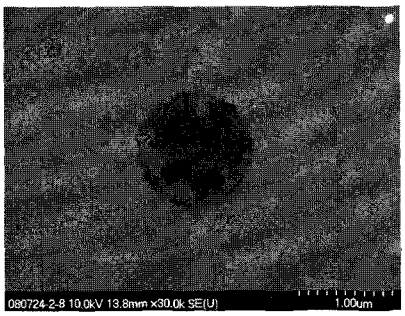

(a)

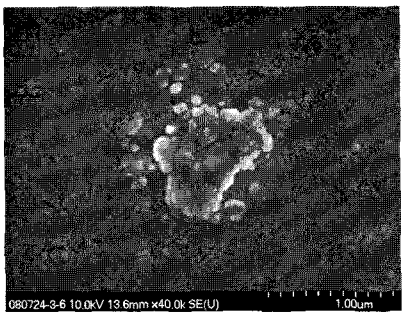

(b)

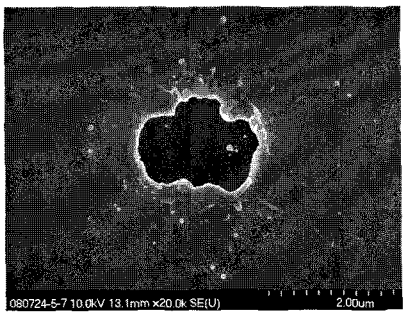

(c)

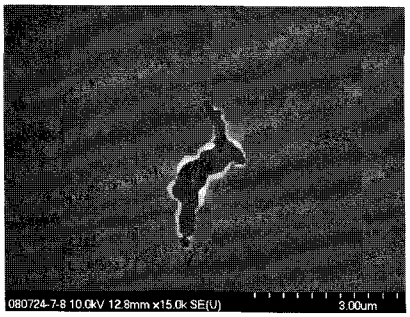

(d)

Fig. 3 SEM images of Au films ablated by 184-fs laser multi (20) pulses. The laser fluences and film thicknesses were (a) 0.995 J/cm^2 for 250 nm (b) 0.926J/cm^2 for 200 nm, (c) 0.712 J/cm^2 for 100 nm, (d) 0.207 J/cm^2 for 20 nm, respectively.

4. Results and discussion

The numerical simulation was conducted for gold for τ_p = 184 fs at the $1/e$ of the maximum intensity and λ = 800 nm. The material and optical properties of gold include, γ = 71 Jm^{-3}K^{-2}, k_{eq} = 318 Wm^{-1}K^{-1}, C_l = 2.5×10^6 Jm^{-3}K^{-1}, G = 2.0×10^{16} Wm^{-3}K^{-1}, R = 0.95 and α = 7.310^7 m^{-1}. At z = 0 and z = d, the adiabatic boundary condition, $\partial T_e(z,t)/\partial z = 0$, is applied with the initial conditions $T_e(z,0)$ = $T_l(z,0)$ = 273 K.

The enhanced model discussed in the section 2 was then applied to the calculation of the damage threshold fluence of gold films under femtosecond laser ablation, where the damage threshold is defined as the laser fluence value at which the lattice temperature reaches the melting temperature (1337 K). In Fig. 4, the damage threshold calculated using enhanced model is shown as a function of film thickness with the experimentally-measured values. Only single-pulse irradiation is assumed for the calculation, whereas both single-pulse and multi-pulse ablation were conducted in the experiments. The damage threshold fluence showed linear behavior with film thickness in the conventional model like 0.14 J/cm^2 for 20nm and 1.54 J/cm^2 for 300nm [20], whereas the trend of damage threshold in the enhanced TTM calculation results is in agreement with the single-pulse experimental data; a similar trend of behavior was also reported by Stuart et al.[3] for the ablation of gold films with λ = 1053 nm and τ_p = 600 fs pulses, thereby supporting the accuracy of the enhanced model over the conventional model.

In spite of the good agreement in trends between enhanced TTM data and single-pulse ablation results, the magnitudes of the values predicted by enhanced model calculation in Fig. 4 are largely different from those measured in the single-pulse ablation experiments. This difference is associated with the uncertainty in detecting ablation marks from experimental targets and also with the definition of damage threshold adopted in the calculation. As explained in Section 3, the damage threshold for the single-pulse ablation experiment was determined by carefully examining a morphological change on the target surface with a SEM after each laser irradiation. Weak damage by a single pulse, however, is very difficult to detect and a visible ablation mark may be found only after the ablation is somewhat significant, thus resulting in higher threshold values. In Fig. 4, the measured threshold fluence is the value at which clear damage was visible on the samples; the error bars represent the fluence range where an emission occurred but visible damage was difficult to locate.

To get rid of this difficulty in damage detection in single-pulse experiments, multi-pulse irradiation may be employed so that the damage accumulates the damage is amplified and more easily detectable. In this case, it is expected that the damage threshold will decrease. Figure 4also shows the experimentally-measured damage threshold for multi-pulse ablation, based on 20 pulses for

each spot. When multi-pulse ablation was adopted, the threshold value decreased by approximately 10-20 %. When the boiling temperature[1] (3081 K) is selected as a definition of damage threshold rather melting temperature[6,15], the curve shifts to higher values, as shown in Fig. 4, almost reaching the values obtained for the single-pulse experiment. As a result, the damage threshold should beunderstood as lying within the band formed by the curves obtained from calculations using the melting temperature (lower limit) and boiling point (upper limit) as definitions of the damage threshold.

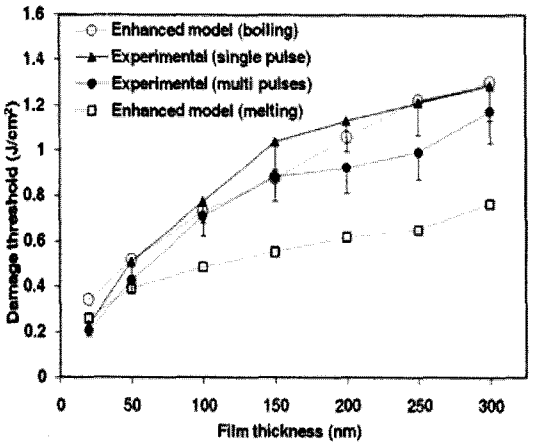

Fig. 4 Damage threshold values calculated by the enhanced model and measured experimentally (Ti:sapphire laser, single pulse ablation, τ_p = 184 fs, λ = 785 nm).

5. Conclusions

We proposed an enhanced TTM for calculating ultrashort pulse laser ablation in which high temperature thermal properties and transient optical properties were used. The predicted damage threshold of gold films showed a clear improvement as compared to a conventional model and closely agreed with the trend of experimentally-measured values. It was also found that the magnitude of the experimentally-observed threshold fluence can be better predicted if the boiling point is adopted as the damage definition in the simulation.

References

1) S. Preuss, E. Matthias, and M. Stuke, "Sub-picosecond UV-laser ablation of Ni films," Appl. Phys. A, **59**, 79-82 1994.
2) S. Preuss, A. Demchuk, and M. Stuke, "Sub-picosecond UV laser abltion of metals," Appl. Phys. A, **61**, 33-37, 1995.
3) B. C. Stuart, M. D. Feit, S. Herman, A. M. Rubenchik, B.W. Shore, and M.D. Perry, "Optical ablation by high-power short-pulse lasers," J. Opt. Soc. Am. B, **13**, 459-468, 1996.
4) S. Nolte, C. Momma, H. Jacobs, A. Tunnermann, B. N. Chichkov, B. Wellegehausen and H. Welling, "Ablation of metals by ultrashort laser pulses," J. Opt. Soc. Am. B, **14**, 2716-2722, 1997.
5) S. I. Anisimov, B. L. Kapeliovich, T. L. Perel'man, "Electron emission from metal surfaces exposed to ultrashort laser pulses," Sov. Phys. JETP **39**, 375-377, 1974.
6) S. S. Wellershoff, J. Hohfeld, J. Gudde, and E. Matthias, "The role of electron-phonon coupling in femtosecond laser damage of metals," Appl. Phys. A, **69**, S99-108, 1999.
7) T. Q. Qiu and C. L. Tien, "Short-pulse laser heating on metals," Int. J. Heat Mass Transfer., **35**, 719-726, 1992.
8) J. K. Chen and J. E. Beraun, "Numerical study of ultrashort laser pulse interactions with metal films," Numerical Heat Transfer, Part A **40**, 1-20, 2001.
9) N. W. Ashcroft, and N. D. Mermin, "Solid state physics," (Brooks/Cole, USA, 1976).
10) C. Kittel, Introduction to solid state physics, (Wiley, New York, 1996).
11) V. Schmidt, W. Husinsky, and G. Betz, "Ultrashort laser ablation of metals: pump-probe experiments, the role of ballistic electrons and the two temperature model," Applied Surface Science, **197-198**, 145-155, 2002.
12) K. Vestentoft and P. Balling, Appl. Phys. A **84**, 207-213, 2006.
13) J. K. Chen, W. P. Latham and J. E. Beraun,

"The role of electron-phonon coupling in ultrafast laser heating," J. of Laser Applications **17**, 63-68, 2005.

14) S. I. Anisimov and B. Rethfeld, "On the theory of ultrashort laser pulse interaction with a metal," Proc. SPIE **3093**, 192-203, 1997.
15) L. Jiang, and H. L. Tsai, "Improved two-temperature model and its application in ultrashort laser heating of metal films," J. of Heat Transfer **127**, 1167-1173, 2005.
16) C. Kittel and H. Kroemer, Thermal physics (W.H. Freeman Company, New York, 1980).
17) M. Fox, Optical properties of solids (Oxford university press, 2001).
18) J. M. Liu, "Simple technique for measurements of pulsed Gaussian-beam spot sizes," Optics letters, **7**, 196-198, 1982.
19) J. Bonse, J.M. Wrobel, J. Krüger, W. Kautek, "Ultrashort-pulse ablation of indium phosphide in air," Appl. Phys. A **72**, 89-94, 2001.
20) T. Balasubramani, S. H. Kim, S. H. Jeong, "Calculation of ultrashort pulse laser ablation of gold films using a quasi-quantum two temperature model," submitted to Appl. Phys. A.